Novel fabrication of Ni_3S_2/MnS composite as high performance supercapacitor electrode

Xiao Huang[a], Zhiguo Zhang[a], Huan Li[a], Yingyuan Zhao[b], Hongxia Wang [c], Tingli Ma[*a,b]

[a] *Department of Life Science and System Engineering, Kyushu Institute of Technology, Kitakyushu 8080134, Japan. Email: tinglima@life.kyutech.ac.jp*

[b] *School of Petroleum and Chemical Engineering, Dalian University of Technology, 124221, China.*

[c]*School of Chemistry, Physics and Mechanical Engineering, Science and Engineering Faculty, Queensland University of Technology, Brisbane, QLD 4001, Australia.*

Abstract:

A Ni_3S_2/MnS composite with unique 3-D morphology was synthesized by a novel method consisting of etching and pre-oxidation of Ni foam followed by in situ hydrothermal method. The etching process created a flower-like structure with the Ni foam which was not only used as a substrate but also providing Ni source for subsequent growth of Ni_3S_2 and Ni_3S_2/MnS composite. The synthesized material showed hierarchical structure consisting of porous Ni_3S_2 which was coated with vertically grown MnS nanorods. The superior morphology enables the access of more active sites in the electrochemical charge/discharge process. In the meantime, the charges involved in redox reaction can be effectively transferred via Ni_3S_2 with relatively high conductivity to Nickel foam substrate, which improved the availability of MnS. Therefore, when the Ni_3S_2/MnS composite was used as a supercapacitor electrode, it showed a remarkable electrochemical performance of 6.70 mAh cm^{-2} which is over two-fold higher than that of the Ni_3S_2 (3.15 mAh cm^{-2}) and MnS (2.34 mAh cm^{-2}) at current density of 2 mA cm^{-2}, respectively. Impressively, the specific capacity of Ni_3S_2/MnS still retained 6.41 mAh cm^{-2} with the capacity retention of 96.5% even after 1000 cycles. Further, the electrochemical properties of asymmetric supercapacitors (ACSs) deliver a maximum energy density of 0.47 mWh cm^{-2} at power density of 10 mW cm^{-2}, together with 82.1% retention after long-term test.

Keywords: In-situ fabrication; Ni_3S_2/MnS composite; stability; supercapacitor.

1 Introduction:

The increasing world population and the application of electronic devices put forward new challenges for clean and safe energy storage systems [1−5]. Among various energy conversion and storage devices, supercapacitors as a promising energy storage system have drawn increasingly public attention due to their high power density, good safety, relatively high capacity and superior cycling durability compared to other types of energy storage systems such as batteries [5, 6]. According to the charge storage mechanism in the electrochemical processes, there are two distinct families of supercapacitors: electrical double-layer capacitors (EDLCs) that take advantage of the charge storage of ion adsorption/desorption and pseudo-capacitors that rely on charge storage involving fast faradaic redox reactions at the electrode/electrolyte interface surface [5]. Consequently, the energy storage capacities of the pseudo-capacitors are much higher than those of EDLCs. The main materials for EDLCs are carbon materials, while transition metal oxides/sulfides with variable valence state have been widely explored as materials for pseudo-capacitors [8−13]. Metal sulfides such as MnS, NiS, Ni_3S_2, CoS, CuS, MoS_2 and WS_2 have been reported to exhibit excellent electrochemical performance due to their good conductivity and higher electrochemical activities [14-19]. Furthermore, metal sulfides possess good mechanical stability when used in the supercapacitors. Among the transition metal sulfides, the inexpensive manganese and nickel sulfides offer incomparable electrochemical performance. Nickel sulfides contain several different types of compound such as NiS_2, Ni_3S_4, Ni_3S_2, α-NiS, β-NiS, Ni_9S_8, Ni_7S_6, etc. Among them, Ni_3S_2 has been reported to possess promising performance as an electrode for supercapacitors. Ni_3S_2 with Specific capacity up to 1.74 F cm^{-2} and 1315 F g^{-1} at 1 A g^{-1} was reported previously [15, 20, 21]. Meanwhile, high energy density supercapacitors based on MnS-based device were also demonstrated previously (about 37.6 Wh kg^{-1}) [14, 22]. Since the performance of supercapacitors strongly relies on the active surface exposed for the redox reactions, preparation of nanostructured materials with high specific surface available for redox reactions and a short diffusion length for the ions and electrons is critical to achieve supercapcatiors with both high energy and high power density [6, 7, 23, 24].

In this study, we developed a new method to synthesize nanostructured Ni_3S_2/MnS composite by a facial in-situ hydrothermal approach combined with etching and pre-oxidization process. The etching of Ni foam by NH_4F was found to create a high surface substrate, which acted a template for the formation of porous structure with the composite. The method has the following advantages. Firstly, the pre-treated Ni foam had much more surface area available for in situ growth of nanostructured Ni_3S_2 and MnS in the hydrothermal reaction. The porous structure was maintained even after the hydrothermal reaction which was favoured for charge transfer with OH^- ions in the charge/discharge process. Secondly, there were no binders or conductive agents involved in the synthesis process of the electrode, which could significantly reduce the resistance and increase the specific capacity of the electrode material. Thirdly, the MnS nanorods that vertically grown on the Ni_3S_2 material with relative high conductivity can be effectively utilized for energy storage. Owing to the unique hierarchical structure and the synergetic effect of Ni_3S_2 and MnS, the Ni_3S_2/MnS composite delivered a very high specific capacity and good stability. The new material synthesis method may open up a new route for preparation of the metal sulfides based supercapacitor materials.

2 Experimental section

2.1 Preparation of Ni_3S_2

All chemicals purchased from Wako Chemical were of analytical degree and used without any purification.

The Ni foam was washed in acetone, 2 M HCl, ethanol and deionized water (DI water) in sequence in order to remove possible residual inorganic/organics on the surface. The Ni foam was then etched by NH_4F solution (0.15 mol L^{-1}) at 100 ℃ for 5 h through a hydrothermal method (labelled as Ni-NF).

In order to obtain Ni_3S_2 and Ni_3S_2/MnS, Ni-NF substrate (1.5 cm × 1.5 cm) was first subject to oxidation at 500 ℃ for 1.5 h (named as Ni-NF-O). Then, the Ni-NF-O was transferred into a Teflon-lined stainless steel autoclave containing Na_2S aqueous solution (0.1 g Na_2S was dissolved in 60 mL DI water) and

$Na_2S/MnCl_2·4H_2O$ solution (0.2 g for Na_2S, 0.1 g for $MnCl_2·4H_2O$ dissolved in /60 mL DI water), respectively. After hydrothermal reaction at 160 ℃ for 12 h, the autoclave was cooled to room temperature, and Ni_3S_2 and Ni_3S_2/MnS composite grafted on Ni-NF substrate were collected.

All the prepared samples were washed 3 times by DI water and ethanol and dried at 60 ℃ in a vacuum oven for 12 h before being tested.

2.2 Materials Characterization

The crystalline structures of the samples were characterized by X-ray diffraction (XRD; RIGAKU) and the morphology was investigated by scanning electron microscopy (FE-SEM, Hitachi 5200). The microstructure and chemical composite of the material were analyzed by high resolution-transmission electron microscopy; (HR-TEM, Tecnai G2 F20 S-TWIN (200KV) equipped with EDX (Energy-dispersive X-ray spectrum). X-ray photoelectron spectroscopy (XPS, KRATOS) was used to verify the chemical composition and the valence states of elements in the material.

2.3 Electrochemical Measurement

The electrochemical measurements were performed in a traditional three-electrode cell. The as-synthesized sample on Ni foam was cut into 1 cm × 1cm pieces and directly used as the working electrode. A platinum net (Pt, 2 cm × 2cm) served as the counter electrode and Hg/HgO electrode acted as the reference electrode. Ni_3S_2/MnS and AC (activated carbon) were used as positive and negative electrode to assemble ASCs, presented in Supporting Information. Prior to the electrochemical test, the samples immersed in 50 mL of a 3 M KOH electrolyte solution were vacuum treated for 30 min at room temperature.

With the 3-electrode system, cyclic voltammograms (CV) tests and galvanostatic charge-discharge (GCD) performance were carried out with the potential window of 0~ 0.6 V and 0~ 0.5V, respectively. Electrochemical impedance spectra (EIS) were

implemented using a Solartron electrochemical station (1287 and 1255B connected) between 1MHz and 10 mHz at AC amplitude of 10 mV.

3. Results and discussion

The scheme in Fig. 1 shows the typical fabrication process for the materials in this work and the obtained structure of Ni_3S_2, MnS and Ni_3S_2@MnS on Ni-NF substrate. The morphology of Ni-NF is dominated by flower-like porous structure, which is very different from that of pristine Nickel foam, as shown in Fig. S1(a, b). After being subjected to oxidation, the pore wall of the pores becomes thicker. However, the Ni-NF-O still possesses the porous feature, which is confirmed in Fig. S1(c). Finally, MnS is vertically and orderly grown on Ni_3S_2 by one-step hydrothermal reaction. However, when the Ni-NF was used as substrate, randomly distributed MnS nanorods was obtained.

The XRD patterns of the as prepared Ni_3S_2, MnS and Ni_3S_2/MnS composite are depicted in Fig. 2. The XRD spectra of three sharp peaks around 45.1°, 52.4° and 76.8° are attributed to the Ni foam. The diffraction peaks at 21.6°, 31.7°, 37.8°, 50.1°, and 55.2° of Ni_3S_2 sample belong to the (101), (110), (003), (113), and (122) planes of Ni_3S_2 respectively (JCPDS No. 44-1418) [13, 15, 20, 21, 25]. The absence of other peaks indicates the purity of the synthesized material. Sharp peaks located at 31.7°, 35.0°, 38.4°, 50.3°, 50.7°, 55.2°, 69.6°, 73.4°, and 78.3° are observed in the XRD pattern of the as-synthesized MnS material, which match well with the diffraction of (111), (200), (102), (220), (103), (201), (203), (210), and (105) facets of MnS, respectively [14, 22, 26, 27]. Meanwhile, all the XRD peaks in the composite can be ascribed to either MnS or Ni_3S_2. Therefore, it is reasonable to conclude that Ni_3S_2@MnS composite was fabricated.

XPS was performed to further verify the composition and elemental valence states of the Ni_3S_2/MnS composite. The typical survey spectrum of Ni_3S_2/MnS

composite is shown in Fig. 2(a), indicating the existence of Ni, Mn, O, C, and S elements. In Fig. 2(b), the two main peaks centred at 855.2 eV and 872.8 eV are assigned to Ni $2p_{3/2}$ and Ni $2p_{1/2}$ accompanied by distinct satellite peaks. The splitting between the two peaks is 17.6 eV, suggesting the coexistence of Ni^{2+} and Ni^{3+} according to previous reports [19, 23, 25, 28]. The peaks at 641.5 eV and 653.0 eV in the high-resolution XPS spectrum (Fig. 2(c)) are indexed to Mn $2p_{3/2}$ and Mn $2p_{1/2}$, respectively [14]. The binding energy at 161.6 eV and 162.5 eV of S corresponds to S 2p3/2 and S 2p1/2. In addition, the peak at 167.8 eV is observed, which suggests that partial S^{2-} was oxidized to sulfate [14, 19, 25]. Therefore, the XPS spectrum reveals that the composite was successfully synthesized, which is in good agreement with XRD.

Before evaluating the electrochemical performance of Ni_3S_2, MnS and Ni_3S_2@MnS, their structure and morphology were characterized by FESEM. As shown in Fig. 3(a-b), the morphologies of Ni_3S_2 and MnS are very different. Ni_3S_2 has a relative smooth surface with many small pores. In order to gain understanding of the morphology evolution of Ni_3S_2, the SEM of Ni-NF substrate and oxidized Ni-NF were monitored. As shown in Fig. S1, the Ni foam etched by NH_4F shows flower-like structure consisting of thin nanosheets, which is expected to effectively increase the surface area of the material. The pore walls of the flower become thicker with sunken holes after oxidization, (Fig.S1f,). Compared to the NiO, the subsequent sulfuration does not dramatically change the morphology of the material except a rougher surface with protuberance (Fig. 3(c)). The porous structure is produced to provide more effective sites for in situ growth of MnS material during the hydrothermal process. As exhibited in Fig. 3(b, d), agglomerated MnS nanorods are randomly distributed on the Ni-NF foam skeleton.

In contrast the MnS nanorods are vertically grown on the Ni_3S_2 surface without agglomeration as shown in Fig. 4(a, d). This is attributed to the in situ induction force of Ni_3S_2. Due to the unique structure, the MnS in the composites should have more effective active sites for the electrochemical

reaction. The charges involved in the redox reaction can be effectively transferred via the relatively high conductive Ni_3S_2, which benefits the electrochemical performance when compared to individual material. In order to investigate more detailed microstructure and the chemical composition of the composite sample, the as-synthesized Ni_3S_2/MnS were further measured by TEM and EDX. It can be seen in Fig. 4(b, e) that small MnS nanorods could be clearly observed in the composites. In addition, selected areas are highlighted by using red lines. The relative dark regions could be indexed to Ni_3S_2 and MnS. Notably, the high-resolution magnification of an area (red circle) in the dark region in Figure 4(b) confirms the existence of nanorods, which is consistent with the results in Fig.4(d). The HR-TEM image of Fig. 4(c) confirms that Ni_3S_2 and MnS are well crystallized. The observed fringe spacing of 0.28 nm and 0.41 nm correspond to the (110) and (101) crystal plane of Ni_3S_2 respectively, while the lattice spacing of 0.31 nm is consistent to the (111) interplanar spacing of MnS [13, 24, 29]. The selected area electron diffraction (SAED) pattern shown in the inset of Fig. 4(f) indicates the polycrystallinity nature of the Ni_3S_2 and MnS. The EDX spectrum shows the existence of Ni, Mn and S, which further confirms the successful preparation of the Ni_3S_2 and MnS. The signals of C and Cu are attributed to the copper grid.

The electrochemical behaviour of the samples was evaluated by CV at a scanning rate of 50 mV s^{-1}. As shown in Fig. 5(a), it is observed that all the samples possess a pair of redox peaks, which is different from EDLCs based material. It suggests the energy storage of the material should come from the Faradaic reaction [6, 19]. Compared to Ni_3S_2 and MnS, the Ni_3S_2/MnS composite show the largest area in the CV plot, indicating its highest capacity. The above results can be verified by GCD patterns at 2 mA cm^{-2}. The composite has the longest discharge time reaching to 900 s whereas the discharge duration of Ni_3S_2 and MnS is only 475 s and 275 s, respectively, confirming the highest capacity of the composite.

In order to further study the reversibility and rate capability of the as-synthesized Ni_3S_2, MnS and Ni_3S_2/MnS, the CV and GCD plots were measured at different scanning rates and current densities. The CV patterns are illustrated in Fig. 6(a, b) and Figure S3. Similar to Fig. 5(a), all the CV curves contain redox peaks, implying the faradaic feature. The redox peaks of Ni_3S_2@MnS can be indexed to those of individual Ni_3S_2 and MnS. Moreover, the responding current densities increase with the increased scanning rates and the composite displays higher current densities at the same scanning rate. Meanwhile, it is noticed that the anodic peaks shift to more positive voltage while the cathodic peaks shift to much more negative voltage with the increase of the scanning voltage rate, which is caused by the kinetics of the interfacial reaction and the sluggish rate of the ionic and electronic transport [15]. The reversible electrochemical reactions are proposed in the following [15, 22]:

$$Ni_3S_2 + 3OH^- \leftrightarrow Ni_3S_2(OH)_3 + 3e^- \quad (1)$$

$$MnS + OH^- \Leftrightarrow MnSOH + e^- \quad (2)$$

$$MnSOH + OH^- \Leftrightarrow MnSO + H2O + e^- \quad (2)$$

Fig. 6(c-d) and Fig. S3(b) are the discharge patterns of the synthesized Ni_3S_2, Ni_3S_2/MnS and MnS at various current densities of 2, 5, 10, 20, 30, 40, and 50 mA cm^{-2}. A plateau is distinctly observed in the discharge curves due to the electrochemical and concentration polarizations [30]. The discharge time of the Ni_3S_2/MnS is longer than that of individual Ni_3S_2 and MnS under the same current density. Finally, the discharge curves are used to calculate the specific area capacity according to the following equation:

$$Cs = I \times \Delta t$$

(Cs: specific capacity; I: current density; Δt: discharge time,).

The specific area capacity as a function of discharge current density is employed to investigate the rate capability, as shown in Fig. 7(a). The areal capacity of the Ni_3S_2/MnS composite is 6.7 mAh cm^{-2} at the current density of 2 mA cm^{-2}, while the Cs is only 3.15 mAh cm^{-2} for Ni_3S_2 and 2.34 mAh cm^{-2} for MnS (Fig. S3), respectively. As the discharge density gradually increases, the Cs decreases owing to limited diffusion of OH anions in the electrolyte. This phenomenon is much more pronounced under the higher discharge currents. Nevertheless, the Cs of Ni_3S_2/MnS composite is still 1.89 mAh cm^{-2} even at 50 mA cm^{-2}, much higher than its corresponding counterparts (Ni_3S_2: 1.21 mAh cm^{-2} and MnS: 1.06 mAh cm^{-2}). The results fully prove that the fabricated Ni_3S_2@MnS composite with unique hierarchical structure is an effective way to realize enhanced electrochemical performance compared to the individual sulfide material.

The cycling performance is an important index of the supercapacitor electrode. The cycling stability of Ni_3S_2, MnS and Ni_3S_2/MnS composite was evaluated under continuous charge-discharge measurements at 2 mA cm^{-2}. As shown in Fig. 7(b), there is no obvious decay in the Cs of the Ni_3S_2/MnS in the first 500 cycles. Even after 1000 cycles, the Cs of Ni_3S_2/MnS is 6.43 mAh cm^{-2} with the retention rate of 96.5%. In contrast, the capacity retention of MnS is 71.5% and the Ni_3S_2 is 86.1%. The inset plots in the Fig. 7(b) are the 1^{st}, 2^{nd}, 3^{rd}, 500^{th}, 501^{th}, 502^{th}, 997^{th}, 998^{th}, 999^{th}, and 1000^{th} cycles of Ni_3S_2/MnS. The shape of the charge-discharge curves is nearly unchanged, which agrees with the above results. The cycling performance of Ni_3S_2, MnS, and Ni_3S_2/MnS composite at larger current density is also tested and shown in Fig. S4. When the current density reaches to 10 mA cm^{-2}, the Ni_3S_2/MnS still demonstrates high Cs of 3.65 mAh cm^{-2} while the Cs of Ni_3S_2 and MnS is only 2.39 mAh cm^{-2} and 1.85 mAh cm^{-2} after 1000 cycles. Based on the above results, it is naturally to conclude that the Ni_3S_2/MnS composite possesses high electrochemical performance.

EIS measurements were performed in the frequency range of 10^{6}-10^{-2} Hz under open circuit voltage condition. The impedance spectra were analyzed by the Zview software and the equivalent circuit model used to fit the EIS spectrum is shown in Fig. 8(a), where Rs represents series resistance, Rct is the resistance of charge transfer, CPE is a constant phase elements with double layer capacitance characteristic, Cps is pseudocapacitive element and W is Warburg impedance. The intercept in real part of the Nyquist plot at high frequency (enlarged Nyquist is shown in the inset of Fig. 8(a)) provides the value of Rs and the Rct resistance due to Faradaic reactions corresponds to the diameter of the quasi semicircle in the middle frequency range. The Rct and Rs of the composite are 0.52 Ω and 0.25 Ω, which indicate the contact resistance and charge transfer resistance in the composite electrode is quite low. In the low frequency range, the relatively vertical line observed with the composite suggests good ion /electrolyte diffusion to the surface of electrode [8, 31, 32]. The Bode plot of the Ni_3S_2/MnS composite which demonstrates the evolution of phase angle as a function of the applied frequency is also analyzed. The phase angle of the composite is about 60° instead of 90°, suggesting its capacity mainly comes from the redox reaction between the Ni_3S_2/MnS and OH^- [30, 33]. The impedance modulus versus angle frequency (Fig. 8c) shows a very good linear relationship between lg|Z| and lgω with about a -1/2 slope in the low and medium frequencies, while lg|Z| is constant in the high frequency range. This is consistent with the results in Fig. 8(a) and Fig. 8(b). Asymmetric supercapacitors were constructed and the results were displayed in Fig. S6.

The aforementioned electrochemical properties reveal that, compared to individual Ni_3S_2 and MnS, the Ni_3S_2/MnS composite possesses high specific capacity and rate capability along with good cycling stability when employed as supercapacitor electrode. The superior property can be explained from three aspects: 1) The Ni_3S_2/MnS grown on pre-treated Ni foam has good conductivity. Nickel foam was directly used as substrate and current collector. More

importantly, the in situ converted Ni_3S_2 and grown MnS reduce the contact resistance. Furthermore, no binder and additives was used in the preparation process. 2) The composite on Nickel foam possesses more accessible active sites for the redox reaction. The Nickel foam treated by NH_4F has much more effective surface, ensuring the Ni_3S_2 obtained by oxidation and sulfuration method has larger surface. In addition, the MnS nanorods were vertically grown on Ni_3S_2 surface without agglomeration, guaranteeing MnS has effective surface for OH ions in the same time; 3)The nanostructured composite has shorter charge transfer and ion diffusion distance.

Conclusions

We developed a novel and simple in situ method for the preparation of Ni_3S_2/MnS composite for electrochemical energy storage system. Ni_3S_2 with flower-like structure combined with the rod-like MnS produced superior energy storage performance. As the electrochemical results showed that at charged/discharged at 2 mA cm^{-2}, the initial specific capacity of Ni_3S_2/MnS (6.7 mAh cm^{-2}) was almost two-fold higher than that of Ni_3S_2 (3.15 mAh cm^{-2}) and MnS (2.3 mAh cm^{-2}). After 1000 cycles, Ni_3S_2/MnS composite still retained 96.5% of the initial specific capacity. Asymmetric supercapacitors were constructed and exhibited high power and energy density. The idea of Ni_3S_2 combined with MnS in this work could offer some guidelines to develop more efficient composite material for supercapacitors.

Acknowledgements

This study was supported by a JSPS KAKENHI Grant Number 15K00597 and Takahashi Industrial and Economic Research Foundation Japan

References

[1] X.-P. Gao, H.-X. Yang, Multi-electron reaction materials for high energy density batteries, Energy & Environ. Sci. 3 (2010) 174−189.
[2] J.M. Tarascon, M. Armand, Issues and challenges facing rechargeable lithium batteries, Nature 414 (2001) 359−367.
[3] X. Huang, Q. Qiao, Y. Sun, F. Li, Y. Wang, S. Ye, Preparation and electrochemical characterization of $Li(Li_{0.17}Ni_{0.2}Co_{0.05}Mn_{0.58})O_2$ coated with $LiAlO_2$, J. Solid State Electrochem. 19 (2015) 805−812.
[4] M. Armand, J.M. Tarascon, Building better batteries, Nature 451 (2008) 652−657.
[5] D.P. Dubal, O. Ayyad, V. Ruiz, P. Gomez-Romero, Hybrid energy storage: the merging of battery and supercapacitor chemistries, Chem. Soc. Rev. 44 (2015) 1777−1790.
[6] P. Simon, Y. Gogotsi, Materials for electrochemical capacitors, Nat. Mater. 7 (2008) 845−854.
[7] A.S. Arico, P. Bruce, B. Scrosati, J.M. Tarascon, W. van Schalkwijk, Nanostructured materials for advanced energy conversion and storage devices, Nat. Mater. 4 (2005) 366−377.
[8] S.H. Aboutalebi, A.T. Chidembo, M. Salari, K. Konstantinov, D. Wexler, H.K. Liu, S.X. Dou, Comparison of GO, GO/MWCNTs composite and MWCNTs as potential electrode materials for supercapacitors, Energy & Environ. Sci. 4 (2011) 1855−1865.
[9] H. Zhou, L.S. Zhang, D.Y. Zhang, K. Xi, S.J. Ding, A universal synthetic route to carbon nanotube/transition metal oxide nano-composites for lithium ion batteries and electrochemical capacitors, Sci. Rep 6 (2016) 37752−37762.
[10] Z. Zhang, Y. He, Q. Zhou, C. Huang, X. Zhang, Z. Guo, Y. Gao, J. Liu, Z. Cao, Unique Ni@NiOcore-shell/AC composite for supercapacitor electrodes, Electrochim. Acta 144 (2014) 300−306.
[11] J. Liang, K. Xi, G.Q. Tan, S.J. Ding, J. Lu, Sea urchin-like $NiCoO_2$@C nanocomposites for Li-ion batteries and supercapacitors, Nano Energy 27 (2016) 457−465.
[12] K. Xu, X. Yang, J. Yang, J. Hu, Synthesis of hierarchical Co_3O_4@$NiCo_2O_4$ core-shell nanosheets as electrode materials for supercapacitor application, J. Alloys Comp. 700 (2017) 247−251.
[13] W. Zhou, X. Cao, Z. Zeng, W. Shi, Y. Zhu, Q. Yan, H. Liu, J. Wang, H. Zhang, One-step synthesis of Ni_3S_2 nanorod@$Ni(OH)_2$nanosheet core-shell nanostructures on a three-dimensional graphene network for high-performance supercapacitors, Energy & Environ. Sci. 6 (2013) 2216−2221.
[14] H. Quan, B. Cheng, D. Chen, X. Su, Y. Xiao, S. Lei, One-pot synthesis of α-MnS/nitrogen-doped reduced graphene oxide hybrid for high-performance asymmetric supercapacitors, Electrochim. Acta 210 (2016) 557−566.
[15] Z. Zhang, Q. Wang, C. Zhao, S. Min, X. Qian, One-Step Hydrothermal Synthesis of 3D Petal-like Co_9S_8/RGO/Ni_3S_2 Composite on Nickel Foam for High-Performance Supercapacitors, ACS Appl. Mater. Interfaces 7 (2015) 4861−4868.
[16] K. J. Huang, J. Z. Zhang, Yun Fan, One-step solvothermal synthesis of different morphologies CuS, J. Alloys Comp. 625 (2015) 158−163.
[17] M. Chen, Y. Dai, J.J. Wang, X.H. Yan, Smart combination of three-dimensional-flower-like MoS_2 nanospheres/interconnected carbon nanotubes for application in supercapacitor with enhanced electrochemical performance, J. Alloys Comp. 696 (2017) 900−906.
[18] A. Khalil, Q. Liu, Q. He, T. Xiang, L. Song, Metallic 1T-WS_2 nanoribbons as high conductive electrode for supercapacitor, RSC Adv. 6 (2016) 48788−48791.

[19] H. Wan, J. Liu, Y. Ruan, L. Lv, L. Peng, X. Ji, L. Miao, J. Jiang, Hierarchical Configuration of $NiCo_2S_4$ Nanotube@Ni–Mn Layered Double Hydroxide Arrays/Three-Dimensional Graphene Sponge as Electrode Materials for High-Capacitance Supercapacitors, ACS Appl. Mater. Interfaces 7 (2015) 15840−15847.
[20] H. Huo, Y. Zhao, C. Xu, 3D Ni_3S_2 nanosheet arrays supported on Ni foam for high-performance supercapacitor and non-enzymatic glucose detection, J. Mater. Chem. A 2 (2014) 15111−15117.
[21] K. Krishnamoorthy, G.K. Veerasubramani, S. Radhakrishnan, S.J. Kim, One pot hydrothermal growth of hierarchical nanostructured Ni_3S_2 on Ni foam for supercapacitor application, Chem. Eng. J. 251 (2014) 116−122.
[22] T. Chen, Y. Tang, Y. Qiao, Z. Liu, W. Guo, J. Song, S. Mu, S. Yu, Y. Zhao, F. Gao, All-solid-state high performance asymmetric supercapacitors based on novel MnS nanocrystal and activated carbon materials, Sci. Rep. 6 (2016) 23289−23297.
[23] H. Lin, F. Liu, X. Wang, Y. Ai, Z. Yao, L. Chu, S. Han, X. Zhuang, Graphene-Coupled Flower-Like Ni_3S_2 for a Free-Standing 3D Aerogel with an Ultra-High Electrochemical Capacity, Eletrochim. Acta 191 (2016) 705−715.
[24] M. Wang, Y. Wang, H. Dou, G. Wei, X. Wang, Enhanced rate capability of nanostructured three-dimensional graphene/Ni_3S_2 composite for supercapacitor electrode, Ceram. Int. 42 (2016) 9858−9865.
[25] J. Wen, S. Li, K. Zhou, Z. Song, B. Li, Z. Chen, T. Chen, Y. Guo, G. Fang, Flexible coaxial-type fiber solid-state asymmetrical supercapacitor based on Ni_3S_2 nanorod array and pen ink electrodes, J. Power Sources 324 (2016) 325−333.
[26] K. Qi, R. Selvaraj, U. Jeong, S.M.Z. Al-Kindy, M. Sillanpaa, Y. Kim, C.W. Tai, Hierarchical-like multipod γ-MnS microcrystals: solvothermal synthesis, characterization and growth mechanism, RSC Adv. 5 (2015) 9618−9620.
[27] X. Li, J. Shen, N. Li, M. Ye, Fabrication of γ-MnS/rGO composite by facile one-pot solvothermal approach for supercapacitor applications, J. Power Sources 282 (2015) 194−201.
[28] L. Shen, J. Wang, G. Xu, H. Li, H. Dou, X. Zhang, $NiCo_2S_4$ Nanosheets Grown on Nitrogen-Doped Carbon Foams as an Advanced Electrode for Supercapacitors, Adv. Energy Mater. 5 (2015) 1400977−1400983.
[29] Y. Tang, T. Chen, S. Yu, Morphology controlled synthesis of monodispersed manganese sulfide nanocrystals and their primary application in supercapacitors with high performances, Chem. Commun. 51 (2015) 9018−9021.
[30] Z.G. Zhang, X. Huang, H. Li, Y.Y. Zhao, T.L. Ma, 3-D honeycomb $NiCo_2S_4$ with high electrochemical performance used for supercapacitor electrodes, Appl. Surf. Sci. 400 (2017) 238–244.
[31] P. Tang, L. Han, L. Zhang, S. Wang, W. Feng, G. Xu, L. Zhang, Controlled Construction of Hierarchical Nanocomposites Consisting of MnO_2 and PEDOT for High-Performance Supercapacitor Applications, ChemElectroChem. 2 (2015) 949−957.
[32] J. Yang, X. Duan, W. Guo, D. Li, H. Zhang, W. Zheng, Electrochemical performances investigation of NiS/rGO composite as electrode material for supercapacitors, Nano Energy 5 (2014) 74−81.
[33] M. Zhi, A. Manivannan, F. Meng, N. Wu, Highly conductive electrospun carbon nanofiber/MnO_2 coaxial nano-cables for high energy and power density supercapacitors, J. Power Sources 208 (2012) 345−353.

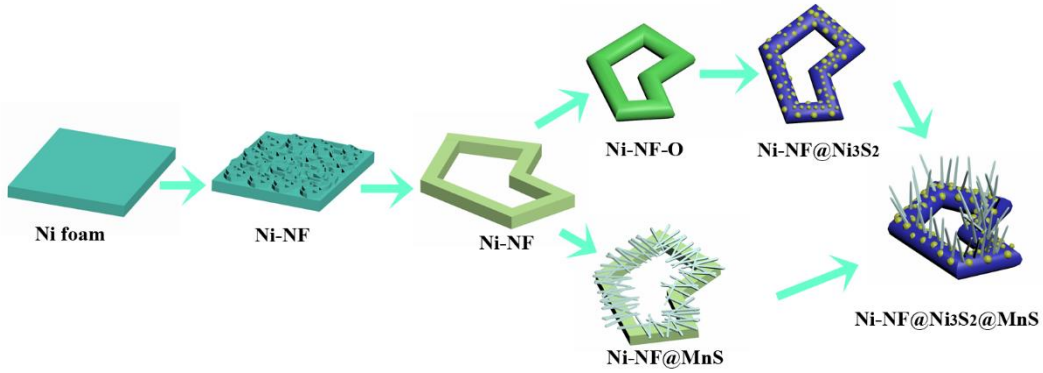
Ni foam
Ni-NF
Ni-NF
Ni-NF-O
Ni-NF@Ni3S2
Ni-NF@MnS
Ni-NF@Ni3S2@MnS

Scheme 1. The procedure for preparation Ni_3S_2, MnS and Ni_3S_2@MnS composite. Note: Yellow sphere represents formation of Ni_3S_2 and nanorods represents MnS material.

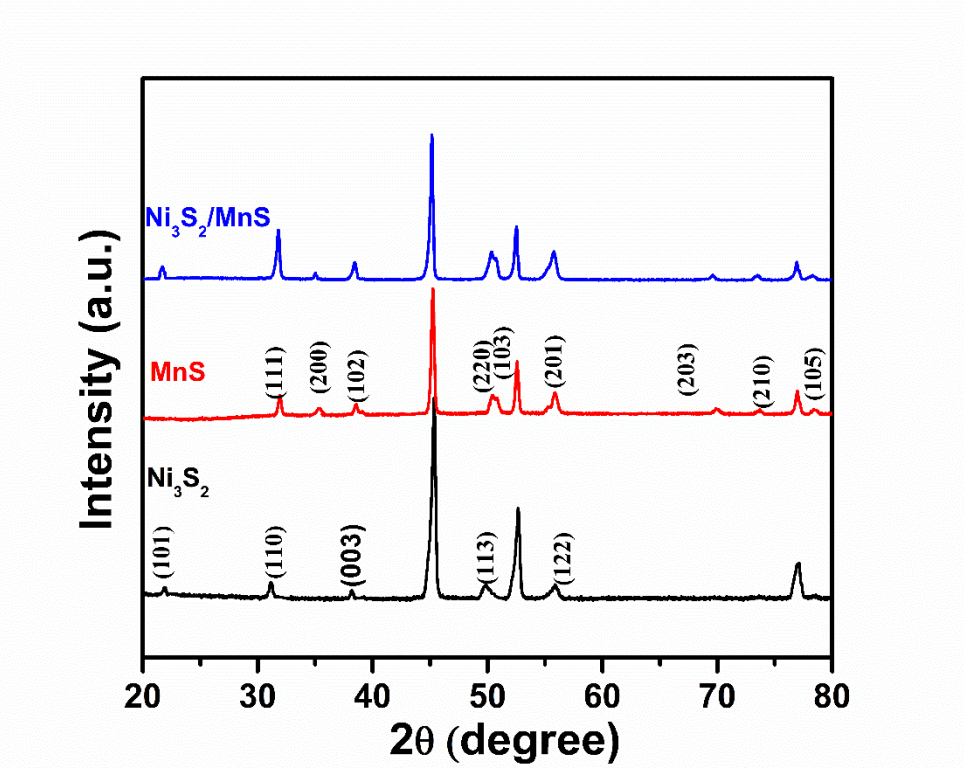

Fig. 1 XRD patterns of Ni_3S_2, MnS and Ni_3S_2/MnS.

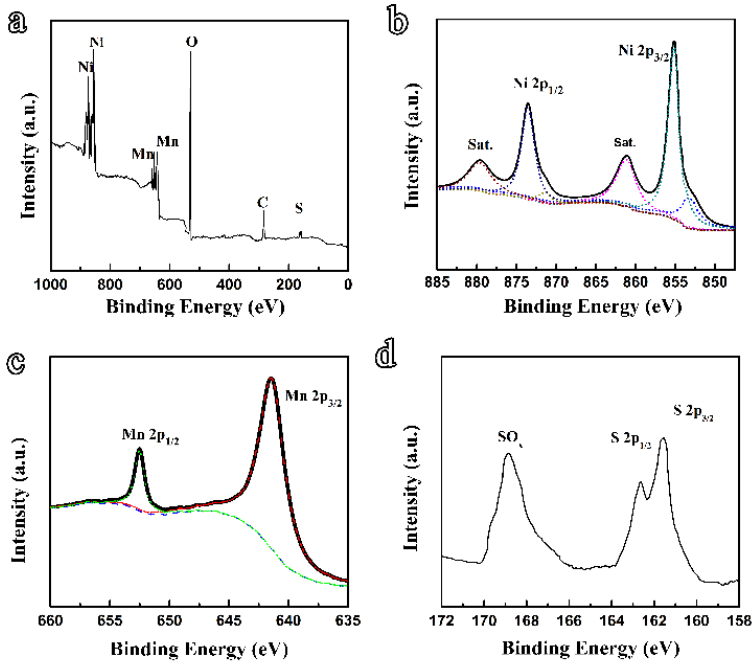

Fig. 2 XPS spectra of Ni_3S_2/MnS composite (a) the survey spectrum, (b) the Ni, (c) the Mn and (d) the S spectrum.

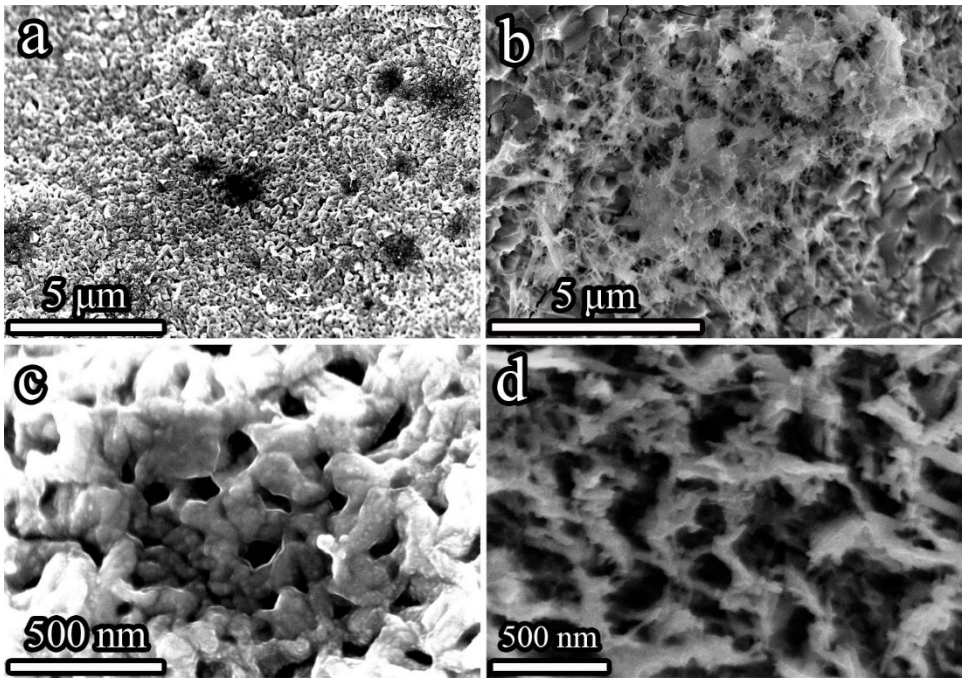

Fig. 3 FE-SEM images of (a, c) the as-synthesized Ni_3S_2 and (b, d) the as-synthesized MnS.

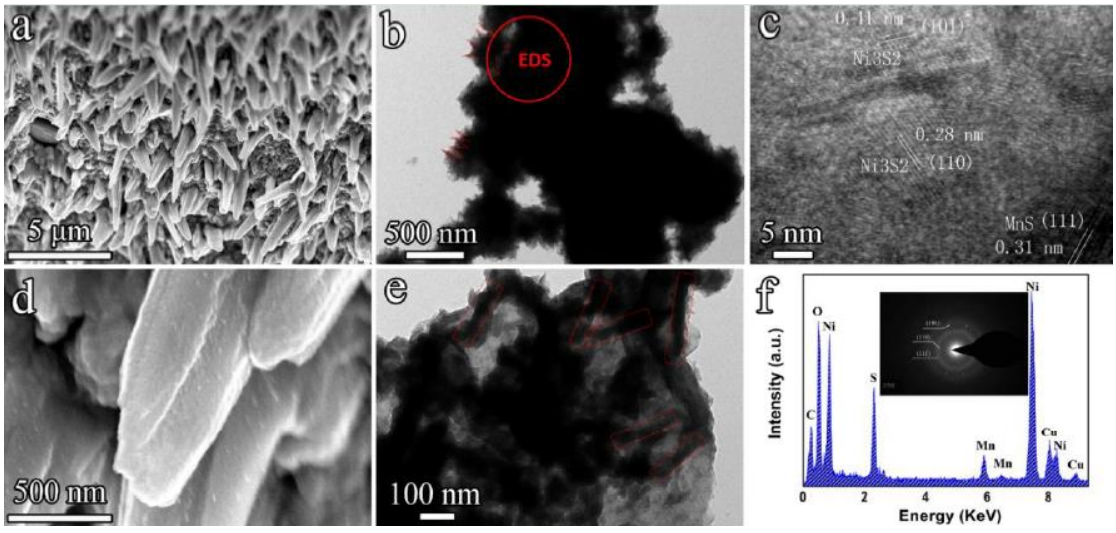

Fig. 4 SEM images (a, d) of Ni_3S_2/MnS composite, morphology (b, e) of Ni_3S_2/MnS characterized by TEM, and HRTEM images (c) of Ni_3S_2 /MnS and EDX spectrum of Ni_3S_2/MnS.

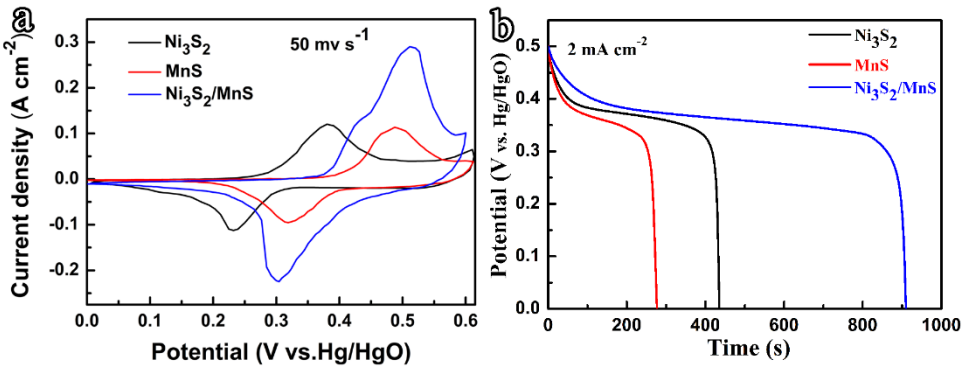

Fig. 5 CV curves (a) and discharge profiles (b) of Ni_3S_2, MnS and Ni_3S_2/MnS composite at current density of 2 mA cm^{-2}.

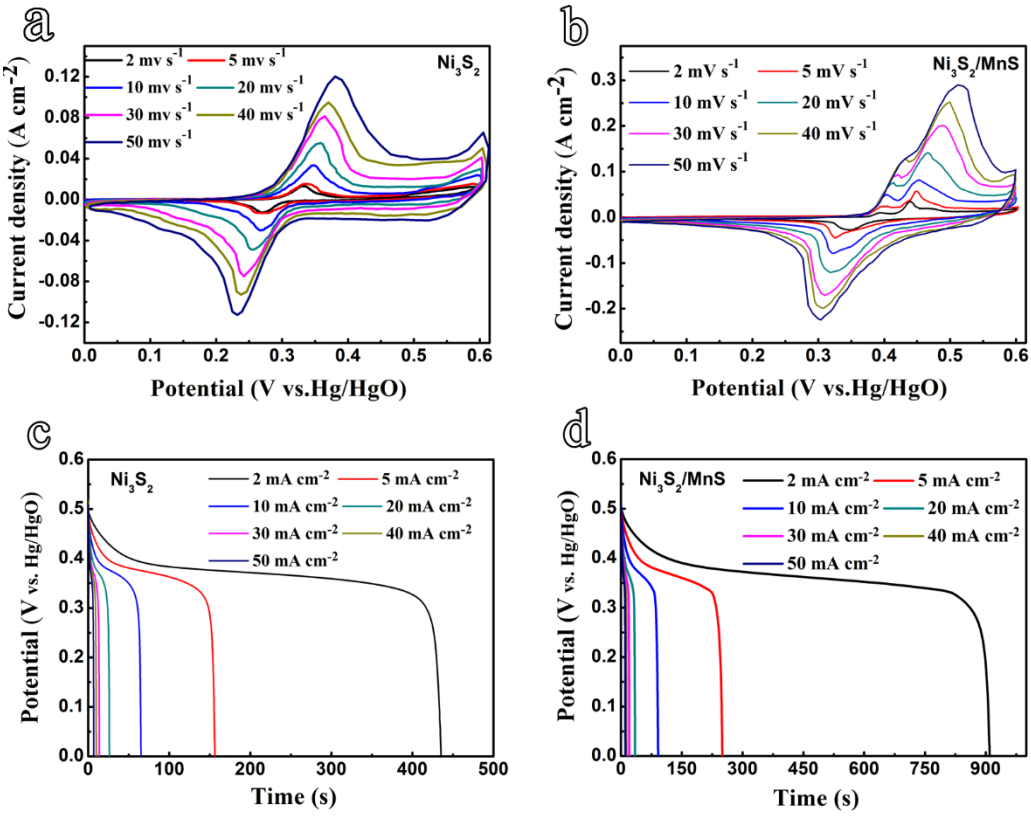

Fig. 6 CV curves of Ni_3S_2 (a) and Ni_3S_2/MnS composite b) at different scanning rates and discharge profiles (c, d) of Ni_3S_2 and Ni_3S_2/MnS composite at different current densities.

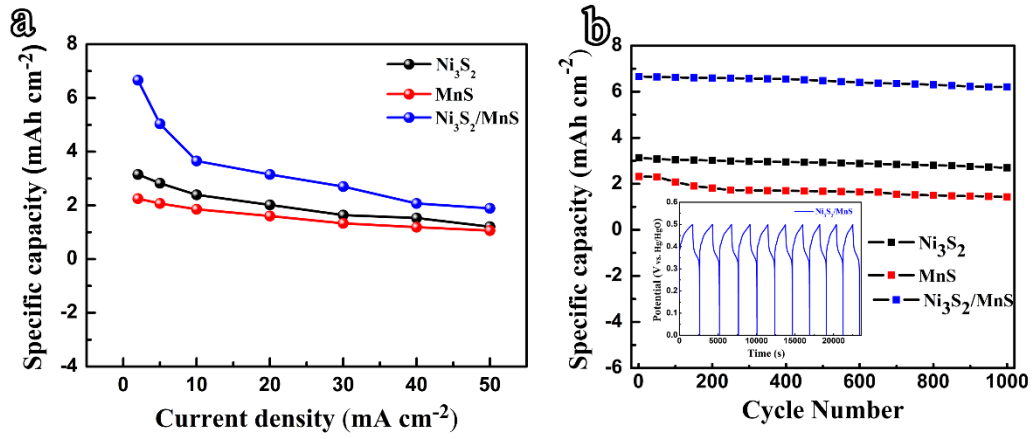

Fig. 7 Specific capacity calculated based on various current densities and cycle performance at 2 mA cm^{-2}.

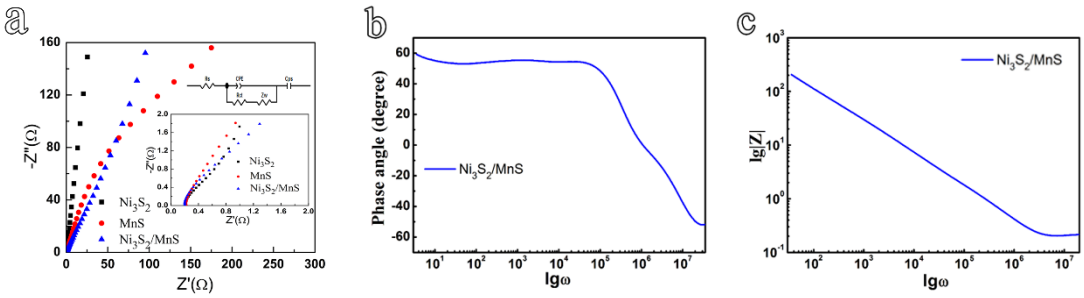

Fig. 8 Nyquist plot (a), phase of impedance versus frequency (b), Bode plot (c) of the Ni_3S_2/MnS composite.